08

Synthesis and morphological properties of graphene on metal and dielectric nanoparticles

© *Yu.A. Salamatov, E.A. Kravtsov, Yu.V. Korkh, Yu.S. Ponosov, M.A. Uimin, D.I. Devyaterikov, M.V. Makarova, V.V. Matyukhov, T.V. Kuznetsova*

M.N. Mikheev Institute of Metal Physics, Ural Branch, Russian Academy of Sciences,
620137 Yekaterinburg, Russia
e-mail: salamatov@imp.uran.ru

Received April 26, 2025
Revised April 26, 2025
Accepted April 26, 2025

The article considers the possibility of applying carbon coatings to nanoparticles by chemical vapor deposition. It has been shown that multilayer graphene can be synthesized on metal and aluminum oxide nanoparticles. It is shown, that carbon films on metal nanoparticles has high structural perfection, despite the significant difference in geometry from planar one. Using a mixture of these nanoparticles, sintering of metal powders can be avoided. The synthesis of carbon coatings on the ensembles of metal nanoparticles, which is formed on a dielectric substrate as a result of thermal coagulation of a thin film, is also analyzed. Such coatings have different morphological properties depending on the thickness of the initial film and the resulting nanoparticle sizes, most often they are multilayer graphene. Raman spectroscopy, atomic force microscopy, X-ray diffraction and reflectometry are used as research methods.

Keywords: nanopowders, carbon coating, thermal coagulatiuon, chemical vapor deposition, Raman spectroscopy, atomic force microscopy, X-ray diffraction, X-ray reflectometry.

DOI: 10.61011/TP.2025.09.61849.81-25

Introduction

In recent decades, there are active studies of properties of nanoparticles of ferromagnetic materials (Fe, Co, Ni) and their alloys. It is shown [1] that depending on intensity of exchange interaction between the particles various magnetic states of their ensemble can be realized and they are termed „supermagnetism“. Application of graphene to metal particles is one of the possible methods of effecting magnetic interaction between them, as a graphene coating changes distances between ferromagnetic cores of the particles and, additionally, graphene also exhibits intrinsic magnetism when there defects in it [2]. Therefore, it can be useful to develop this approach for more detailed study of the supermagnetism phenomena, to which a lot of studies are dedicated (see, for example, [3–5] and references therein). Graphene „isolates“ metal particles from each other, which will enable creating supermagnetic ensembles in bulk powders and not only in systems on a substrate.

The mentioned metals are catalysts of thermal decomposition of hydrocarbons [6]. When these nanoparticles are placed in an atmosphere of the gas that contains hydrocarbons even at small partial pressures, a carbon film is formed on their surface. By changing a gas pressure and a process temperature, it is possible to controllably vary a number of the carbon layers and presence of structural defects in it. However, for nanopowders of ferromagnetic transition metals (Fe, Co, Ni) and their alloys there is quite little experimental data about the change of their properties (including magnetic ones) when applying the carbon covering. The available results are not of a systematic nature: they are usually data for the same specific synthesis conditions, wherein they are for a specific task that is usually an applied one.

It is known, for example, that catalyst activity of Co nanoparticles significantly increases when applying a graphene coating to them [7]. After synthesis of graphene, the very particle can be etched off by hydrochloric acid to leave only the graphene coating — the catalyst activity of these items turns out to be even greater, thereby indicating that the very particle is not directly involved in the processes. It was shown in the study [8] that application of graphene to the nanoparticle contributes to using optical research methods. First of all, it is related to optical transparency of graphene, and, secondly, to the fact that it protects a research item against chemical effects, in particular, against oxidation by atmospheric air. In some cases, it also suppresses effects of fluorescence and photobleaching. The authors [9] have synthesized the FeCo particles in the graphene coating, but the main purpose is application in liquid electrolytes. Only magnetization of saturation of the nanoparticles was measured. The same group carried out deeper research of the sample, but only growth conditions and a number of the graphene layers were included without referring them to properties of the nanoparticles [10]. These studies used ensembles of nanoparticles on an aluminum matrix rather than individual nanoparticles. „Independent“ Fe nanoparticles in the graphene coating were investigated in some studies [11], but mainly as applied to biomedical tasks (delivery of biologically active substances into a

body and their release therein). The nanoparticles in the carbon coatings have an application potential in solving environmental problems, too, in particular, for purifying water by magnetic separation [12,13].

There are several methods of producing both pure and coated nanoparticles. One of these methods is a gas-phase synthesis, which is as follows. A drop of melt metal, which is levitating in the magnetic field, is flowed with a carrying-gas (argon). At the same time, metal vapor is condensed and crystallized to form nanoparticles. When adding oxygen or hydrocarbons into argon (methane, butane, etc.), it is possible to produce nanoparticles of oxides or carbides. It is also possible to encapsulate the metal particles in carbon coatings, which are usually amorphous carbon or graphite [14]. More details about the method can be found in the studies [15–17].

The authors of the study [18] have proposed a method based on thermal decomposition of metal acetates in a hermetic capsule. The same method was used by the same group to try to synthesize bimetal multi-layer nanoparticles in the carbon coating [19].

Another approach to producing the nanopowders is to mechanically grind in ball mills, planetary mills or disintegrators. With impact-abrasion interaction of the initial particles with each other or with a mill mechanism, they are gradually refined to a desirable size. The grinding time depends on a material and a refinement method and is usually from tens to hundred hours [20].

The above-described methods are designed for producing nanopowders in a piled state. It is possible to synthesize the ensemble of the nanoparticles on a substrate [8]. A thin metal film (its thickness does not exceed several hundred angstroms is applied to the dielectric substrate and then it is annealed at the temperature that is close to the melting temperature. Continuity of the metal layer is disrupted and it forms multiple clusters on the initial substrate, whose size depends on the initial thickness of the material.

A convenient method of synthesis of the carbon coatings is chemical vapor deposition. The gas that contains carbon (methane, ethylene, acetylene, butane, etc.) is transmitted through a quartz tube at the high temperature (usually 900 °C–1100 °C). The sample is placed in the same tube. Its surface shall have catalysts properties and facilitate thermal dissociation of the hydrocarbon molecules. The carbon atoms released in this process are adsorbed by a sample surface to form the film thereon. Advantages of the chemical deposition method include applicability of carbon to items of any morphology and its rate (the carbon film is formed for several minutes in case of metal catalysts regardless of the sample size). The disadvantages may be that it is necessary to heat to high temperatures, thereby making the method unsuitable for thermally unstable samples.

The present study includes detailed consideration of the chemical vapor deposition method as a method of synthesis of the carbon coatings on various types of the nanoparticles and specifies a dependence of their structural properties and quality on a type of the initial samples. It proposes various approaches to solving some problems that are typical for this method — sintering of the nanopowders, formation of „spurious“ nonmagnetic phases in the nanoparticles. A dependence of the morphology of the carbon covering on the thickness of the initial metal film is analyzed for the ensemble of the nanoparticles on the substrate. A material of the nanoparticles was selected to be Ni and its alloy $Ni_{81}Fe_{19}$ (permalloy), as nickel is a very effective catalyst for growth of the carbon films.

1. Experiment

The following samples were prepared for the experiments of synthesis of the carbon coatings and investigation of their morphological properties:

1) the Ni foil of the thickness of ~ 0.3 mm;

2) the Ni powder with the average particle size of 53 nm;

3) the planar Al_2O_3 substrate that is cut out in the plane R $(1\bar{1}02)$;

4) the Al_2O_3 nanopowder with the average particle size of 30 nm;

5) the mixture of the nanopowders $Ni + Al_2O_3$ in the ratio 1 : 3 respectively;

6) the thin Al_2O_3//Py(t) films. Here, Py designates a permalloy alloy ($Ni_{81}Fe_{19}$), t = 15, 55, 105, 300, 500 Å is a thickness of the permalloy layer.

The Ni foil and the Al_2O_3 substrates are commercially available. The Ni nanopowder was produced by the gas-phase method in an argon flow without adding other gases in an original facility in the Institute of Metal Physics, Ural Branch of the Russian Academy of Sciences (Yekaterinburg). The pressure in the synthesis chamber is 150 mm Hg. The gas flow rate is 130 l/min. The synthesis of the metal nanopowders includes passivation after their production by gradually supplying air into the synthesis chamber. As a result, the surface of the particles has a thin oxide layer formed to prevent further oxidation (and possible self-ignition) of the powder in its contact with air.

Oxygen is added into the carrying gas for synthesis of the Al_2O_3 nanopowder. Vapor condensation is accompanied by oxidation. As a result of quite fast cooling in transfer of the particles by the gas flow, it is possible to obtain quite big deviation from the stoichiometric metal-oxygen ratio (oxygen shortage). In particular, it is observed for aluminum oxides, whose color can be closer to gray and only after annealing in air at the temperatures above 500 °C–1000 °C the stoichiometric ratio is restored (the powder color is visually changed to white).

The sizes of the nanoparticles were evaluated by results of measurements of a specific surface area by the Brunauer-Emmett-Teller method. After that, for convenience of work, the used nanopowders and their mixture were pressed into tablets of the diameter of 4–5 mm and the thickness of 1 mm. The compaction pressure was 1 t.

The Al_2O_3//Py(t) films were prepared by magnetron sputtering of a target of a respective chemical composition

by argon plasma in the ULVAC installation in the Institute of Metal Physics, Ural Branch of the Russian Academy of Sciences (Yekaterinburg). Sputtering was performed at the room temperature; the base vacuum level in the growth chamber was $5 \cdot 10^{-7}$ Pa, the argon pressure was 0.1 Pa and the growth rate was ~ 0.5 Å/s.

The carbon layers were synthesized in a chemical vapor deposition installation. The installation is equipped with a horizontal quartz glass reactor of a displacement type, which has hot walls. A table is horizontal and does not require additional fixtures for the samples. Methane CH_4 is the carbon source.

Just before being loaded into the reactor, the foil and the Al_2O_3 substrate were flushed in an ultrasonic bath in acetone to remove organic contamination from the surface. Then, they were held in acetic acid, which also dissolves organic traces and, moreover, loosens the oxide layer on the metal surface, thereby contributing to its further removal when annealing. Reagent residuals and mechanical contaminants were finally removed by flushing in deionized water and isopropyl alcohol. The foil and the substrate were dried in a dry nitrogen flow.

The tablets of the nanocrystalline powders were produced by a team of the authors independently in laboratory conditions, therefore they are assumed to be quite clean. It is significantly difficult to flush them, therefore, it was not carried out.

Initially, the carbon covering was simultaneously synthesized on the Ni foil and the pellet of the Ni compressed nanopowder.

The samples were pre-annealed in hydrogen in the reactor to remove an oxide film from the metal surface. The annealing temperature is 1075 °C, the period of time is 30 min, the hydrogen flowrate is 120 cm^3/min and the gas pressure is 10 mm Hg. Annealing functions as additional purification for the aluminum oxide samples.

The synthesis itself was carried out at the temperature of 1035 °C. A mixture of hydrogen and methane was supplied into the reactor, the flowrates were 120 and 5 cm^3/min, respectively, while the pressure was 10 mm Hg. The gas mixture was supplied for 10 min and after that the gas flow was stopped and the furnace was switched off and opened to provide fast cooling of the reactor and the samples. The cooling was carried out at the pure-hydrogen flowrate of 200 cm^3/min under the pressure of 10 mm Hg. When the temperature 300 °C was achieved, hydrogen was cut off, the reactor was purged with argon and then filled with argon to the atmospheric pressure. Further cooldown was performed in argon, the samples were extracted at the temperature below 50 °C.It should be noted that all the provided parameters are optimized for the specific installation, reactor geometry and gas supply scheme. When reproducing the experiments in other installations, it is necessary to select or recalculate the parameters based on their characteristics. The provided values can be used only as approximate ones.

As follows from the phase diagram (see, for example, [21]), at the high synthesis temperature solubility of carbon in nickel is significantly increased. Besides, nickel is a catalyst of thermal decomposition of hydrocarbons. As a result, carbon released during methane decomposition is actively absorbed by the nickel substrate (or the nanoparticles of the Ni powder). During fast cooling (15–20 °C/min) of the sample, upon completion of the synthesis solubility decreases and excess carbon is released on the surface to form graphene, multi-layer graphene or graphite thereon, depending on an amount of dissolved carbon [22]. Amorphous carbon can be formed, but when interacting with hydrogen its nuclei dissociate to form gaseous hydrocarbons, which are removed out of the reactor. Ordered layers are not destroyed due to stronger bonds in a lattice. Consequently, in order to reduce the amount of spurious amorphous carbon on the samples, a hydrogen flow is continuously transmitted through the reactor in the stages of synthesis and cooling.

Aluminum oxide Al_2O_3 (sapphire) is also a catalyst of thermal dissociation of hydrocarbons and can form the graphene film on its surface [23,24]. In this regard, it is interesting to check applicability of the carbon coating to the sapphire nanoparticles. The planar Al_2O_3 substrate (as a reference sample) and the Al_2O_3 nanopowder compressed into the pellet were simultaneously used for the experiment. Differences from the above-described synthesis scheme for the metal include the growth time and the values of the gas flowrates. Since sapphire has considerably weaker catalyst activity, the growth time was 90 min. For the same reason, the hydrogen flowrate was reduced to 50 cm^3/min, while the methane flowrate was increased to 15 cm^3/min — for interaction of the higher number of carbon atoms with the surface.

The carbon coatings were synthesized on the mixture of the nanopowders and on the ensemble of the particles on the substrate in the same scheme as for pure nickel.

2. Results and discussion

2.1. Ni foil and the Ni nanopowder

The produced samples were studied by Raman spectroscopy. The Raman spectra were excited by a line of the wavelength of 532 nm (the photon energy is 2.33 eV) of the solid-state laser. The Raman spectrometers SOL Instruments Confotec MR 200 (the Institute of Metal Physics, Ural Branch of the Russian Academy of Sciences, Yekaterinburg) and Renishaw RM 1000 (the Institute of High-Temperature Electrochemistry of the Ural Branch of the Russian Academy of Sciences, Yekaterinburg) were used. The optical microphoto of the foil surface and the spectra in several points are shown in Fig. 1, *a*.

The microphoto clearly exhibits foil rolling strips and quite large grains (from 3 to 14 μm and 7 μm on average), which were enlarged during recrystallization when

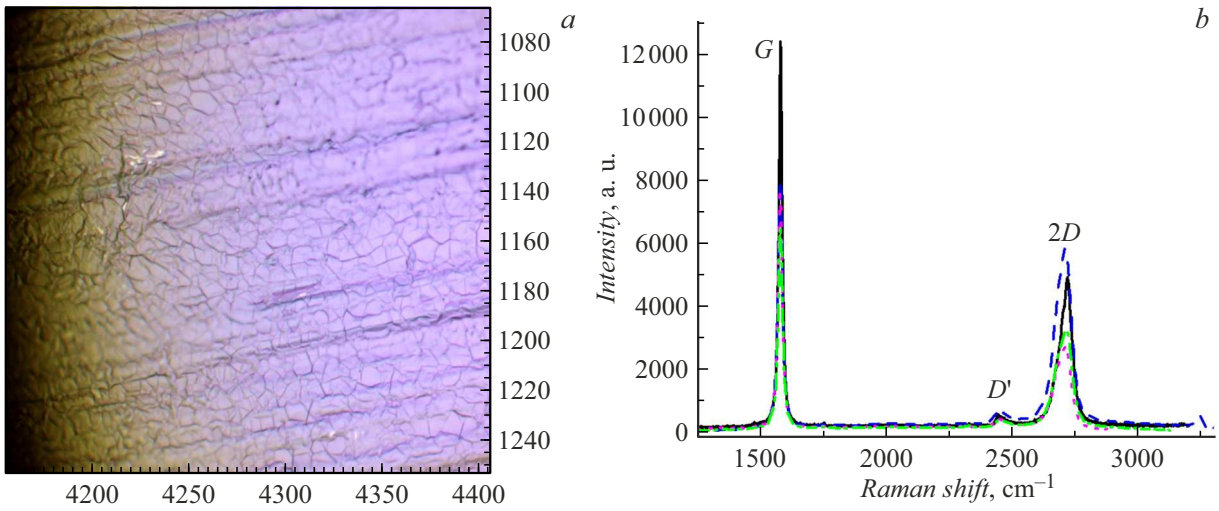

Figure 1. *a* — the optical photo of the surface of the Ni foil (the area $180 \times 250\,\mu m^2$); *b* — the Raman spectra obtained in four different points of the sample.

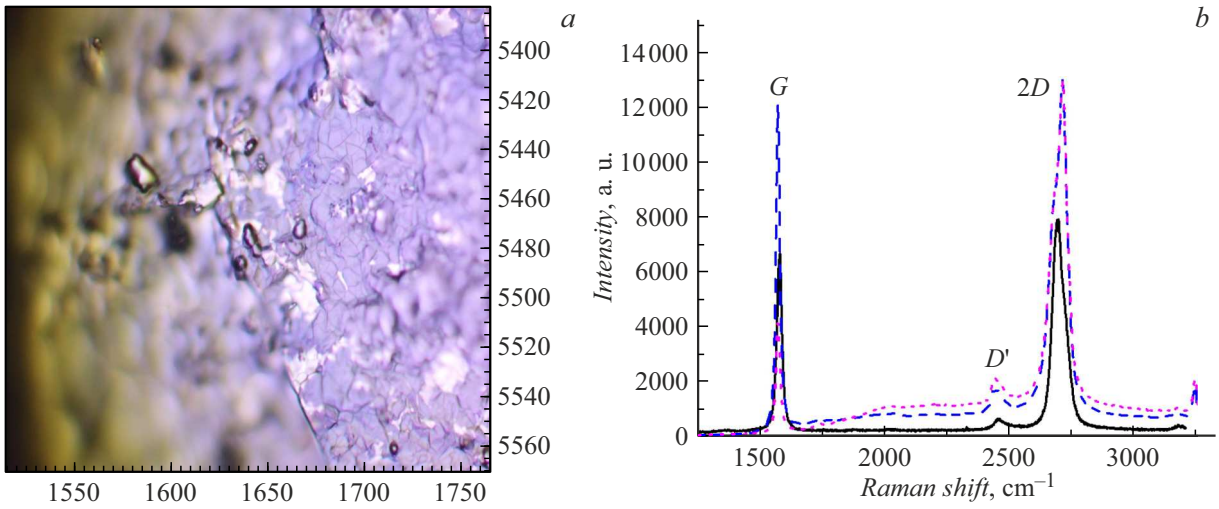

Figure 2. *a* — the optical photo of the surface of the Ni pellet (the area $180 \times 250\,\mu m^2$); *b* — the Raman spectra obtained in three different points of the sample.

annealing. For comparison, the pellet, whose nanoparticles were sintered during the synthesis, has finer grains and no strip (Fig. 2). Several lighter spots are also visible on the pellet. Smeared areas on the microphoto appeared due to the fact that during sintering a pellet surface became uneven and it was not possible to focus on the entire visible range. In accordance with data of the Raman spectra (Fig. 1, *b*), both the samples exhibited the following spectrum lines: *G* ($1575\,cm^{-1}$) — the spectrum line of the first order, which is a longitudinal mode of oscillation of carbon atoms (i.e. the degenerate E_{2g} mode that extends a carbon ring within a plane), 2*D* or *G'* ($2710\,cm^{-1}$) — the spectrum line of the second order (overtone *D*), which is typical for graphene. The mode *D* appears due to disorder-activated double resonance from LO optical branches of the phonon spectrum near a point *K* of the Brillouin area. If the disorder role is played by the second phonon with a large wave vector, then the *G'* mode appears, which is exactly called an overtone of the *D* mode.

A peak ratio I_{2D}/I_G indicates that the multi-layer graphene has been formed on the surface of the nickel foil ($I_{2D}/I_G < 1$, the number of the layers exceeds 3, the same follows from analysis of the FWHM (full width at half maximum) of the peak 2*D*). During the synthesis, the pellet had grey spots (they are in majority) with two-layer ($I_{2D}/I_G > 1$) and, locally, single-layer graphene ($I_{2D}/I_G > 2$) and white spots with single-layer graphene formed on the surface. Some points of the samples have graphite. All the spectra of both the samples have no peak *D*, thereby indicating no disordering, strain and defects in a crystal structure of the carbon layers. The main characteristics of the spectra are shown in Table 1.

Table 1. Characteristics of peaks of the Raman spectra obtained on the samples of the Ni foil and the Ni nanopowder pellet

Substrate	Position of the peak $2D$, cm^{-1}	FWHM of the peak $2D$, cm^{-1}	I_{2D}/I_G
Foil	2710	77–80	0.4–0.7
Pellet			
Grey spots	2710	75	1.07–3.1
White spots	2690	45	3

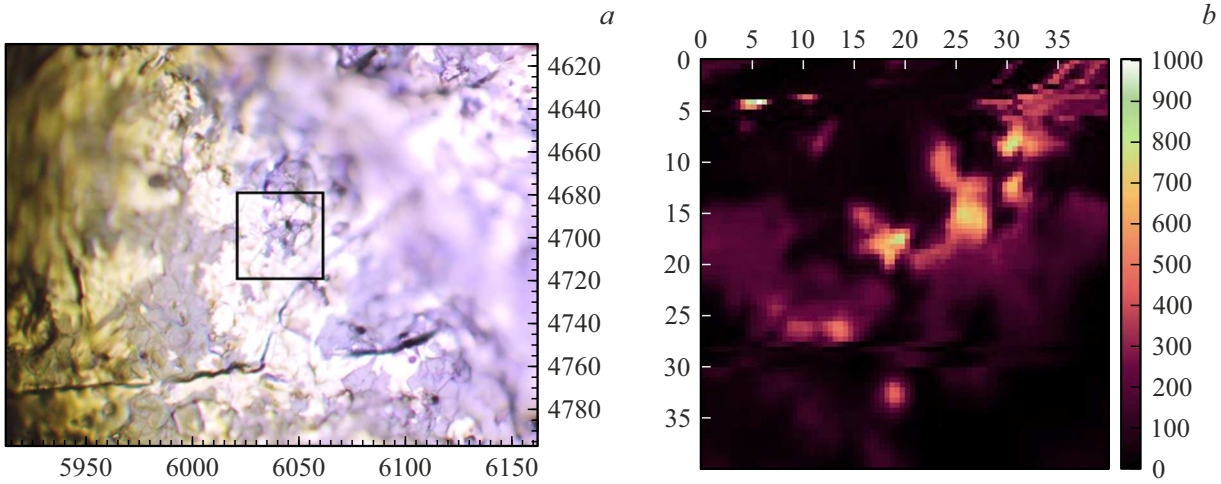

Figure 3. *a* — the optical microphoto of the surface of the Ni pellet ($180 \times 250\,\mu m^2$), the studied area is marked; *b* — the map of distribution of intensity of the peak $2D$ in points of this area.

There is certain ambiguity in interpretation of the Raman spectra for graphene synthesized on nickel. According to the review [25], electron-phonon interaction in this system is altered such that conditions of a resonance required for forming the Raman signal are not satisfied. A signal from graphene is either totally absent or heavily suppressed. Observation of the signal may indicate either presence of multi-layer graphene or weakening of a bond between graphene and nickel due to presence of impurities. Chemically pure nickel was used for the study and the second option looks unlikely. Consequently, hereinafter we will assume that the Raman spectrum that describes graphene on nickel actually corresponds to two-layer graphene.

It is noted in the review [26] that the presence of impurities, mechanical stresses and other factor can result in shift of the Raman peaks, including the possibility of obtaining configurations that are typical for graphene, when several carbon layers are actually in the sample. Unambiguous determination of the number of the layers requires involvement of additional techniques, for example, transmission electron microscopy. The present study investigates morphological characteristics of the carbon coverings that can be characterized as multi-layer graphene (a small number of atomic carbon monolayers). It is just necessary to distinguish them from amorphous carbon and graphite, for which capabilities of Raman spectroscopy are sufficient.

We have obtained for the pellet a map of distribution of intensity of the peak $2D$ ($2700\,cm^{-1}$) across the surface of a studied area of the sample (it is marked by a black rectangle), which characterizes distribution of the number of the carbon layers (Fig. 3). Here, light areas correspond to the grey spots on the surface, the spectra on them show the high peaks G and $2D$, their height ratio corresponds to multi-layer graphene. Dark areas in the map of distribution of the maximums of intensity of $2D$ correspond to the spectra with smaller intensities of all the peaks, but the ratio between G and $2D$ corresponds more to two-layer graphene. So, the lighter spots of the map contain more carbon layers. The map illustrates heterogeneous distribution of the number of the layers across the sample surface. The spots with two-layer graphene prevail. Heterogeneity can be caused by a change of the pellet form during sintering of the nanoparticles, as due to the small size of the sample it was uniformly circumvented by the gas mixture. Besides, a geometry of the nanoparticles can affect, too, as their surface highly differs from planar surfaces of the standard substrates due to the very small size.

It is shown on this series of the samples that synthesis of multi-layer graphene can be on the nickel nanoparticles, wherein the number of the layers on average is less than for the foil that was a reference sample. It can be explained by a small volume of the nanoparticle, which results in dissolution of a small amount of carbon in it. When released

Table 2. Parameters of decomposition of the peaks of the Raman spectrum for graphene on sapphire using the Lorentz function

Position of the peak G, cm^{-1}	I_D/I_G	Position of the peak $2D$, cm^{-1}	FWHM of the peak $2D$, cm^{-1}	I_{2D}/I_G
1582	~ 1.3 high density of defects	2676	63	~ 1.2 $\sim 2-3$ -layer graphene

on the surface during cooling (this surface is quite large in case of the nanoparticle), this amount shall form a smaller number of the layers than in the case of the bulk sample. By selecting the synthesis parameters (the exposure time, the temperature, the gas flowrate ratio), it is possible to achieve formation of graphene, too. The produced coatings have high structural perfection, which is indicated by no peak D on the spectra.

But there is still a problem of sintering of the nanocrystalline nickel powder at the high temperatures that are necessary for the synthesis. This problem will be relevant for the other transition metals that can form carbon films during chemical vapor deposition. To solve it, it was proposed to use a mixture of nanopowders of nickel and aluminum oxide $Ni + Al_2O_3$. Aluminum oxide was selected for the following reasons. First of all, the high melting temperature (above 2000 °C) excludes the possibility of sintering of the oxide nanoparticles and hinders sintering of the nickel nanoparticles. Secondly, aluminum oxide can also form the carbon film on the surface, although it has considerably weaker catalyst activity. First, we have checked synthesizability of the carbon covering on the Al_2O_3 nanoparticles.

2.2. Al_2O_3 substrate and the Al_2O_3 nanopowder

The Raman spectrum for the sapphire substrate after synthesis (Fig. 4) confirms that its surface has the carbon covering with a variable number of the monolayers and high density of the structural defects formed. No peak that corresponds to amorphous carbon is observed. Results of analysis of the spectrum peaks by their approximation with the Lorentz functions are shown in Table 2.

The particles of the Al_2O_3 nanopowder have also a similar covering formed, which is confirmed by the Raman spectrum (Fig. 5). The ratio of intensities of the peaks $2D$ and G indicates presence of $2-3$ carbon monolayers. The large FWHM (full width at half maximum) of the peaks, the high peak D and appearance of the peak D' (near the peak G) are due to a large number of the structural defects. The carbon film on sapphire is formed with generating many nuclei that enlarge and combine with each other, thereby resulting in emergence of a large number of grain boundaries [23]. These are the main source of defects of an atomic lattice of the monolayers. A defectiveness

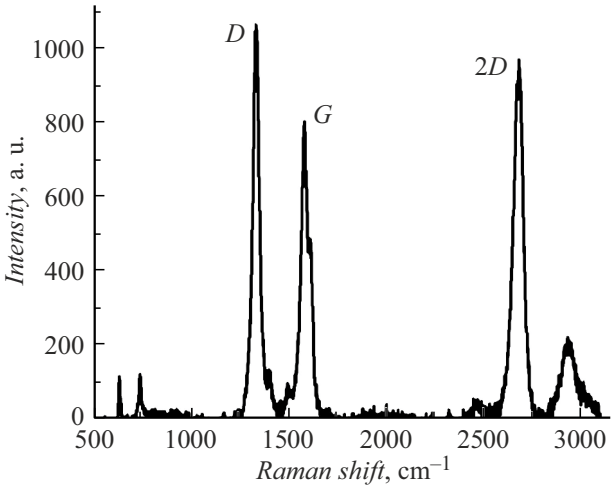

Figure 4. Raman spectrum for the sample of the carbon film that is synthesized on the Al_2O_3 substrate.

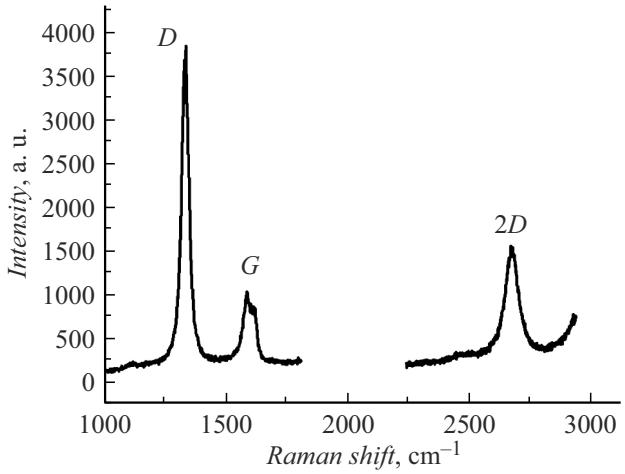

Figure 5. Raman spectrum for the sample of the nanocrystalline Al_2O_3 powder with the carbon covering.

degree depends on a plane, in which the substrate is cut out [24], but the nanopowders can include any possible orientations of the surface, wherein ribs between facets are also a source of defects. Generally, they can originate nuclei of amorphous carbon, too, but they are not observed in our samples. It indicates a correct choice of the value of the

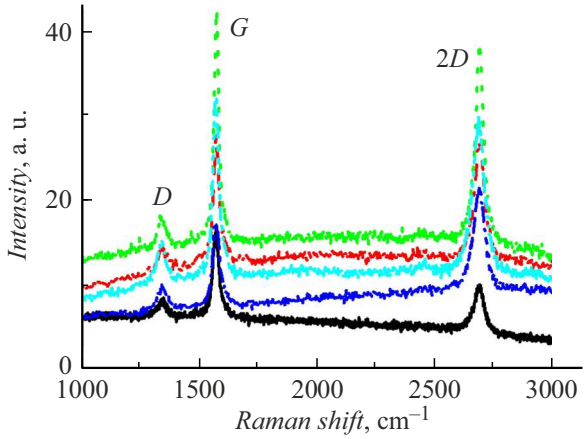

Figure 6. Raman spectra for the sample of the mixture of the nanocrystalline powders $Ni + Al_2O_3$ with the carbon covering. The different curves correspond to the different points on the sample.

hydrogen flowrate during the synthesis, which is enough for destroying amorphous carbon. It is also shown in the study [24] that it is possible to slightly reduce defectiveness of the carbon film on the sapphire substrate by increasing the synthesis temperature.

2.3. Mixture of the nanopowders $Ni + Al_2O_3$

During synthesis of the carbon covering this sample was not sintered. The Raman spectra in several points are shown in Fig. 6.

The ratios of the heights of the peaks $2D$ and G on the presented spectra predominantly correspond multi-layer graphene. The number of the layer is 4–5 in some points. Unlike the previously considered nanopowder of pure nickel, a weak peak D ($\sim 1350\,\text{cm}^{-1}$) is manifested here to indicate that defects are present in the atomic lattice of the carbon layers. Thus, adding the sapphire nanoparticles Al_2O_3 insignificantly worsens the covering quality and increases the number of the layers, but at the same time prevents the nanocrystalline powder from sintering.

It was found during X-ray diagnostics of the powder after synthesis that aluminum oxide is partially reduced. Aluminum was not released in a pure form, but formed a Ni_3Al phase. It was preliminarily estimated that at most 2 % of pure nickel is still present as compared to the initial amount. The Ni_3Al phase is formed during interaction of the powder with methane, since it is not observed after simple annealing in hydrogen. A nature of this phenomenon is not completely clear and requires further detailed research. It should be noted so far that Al_2O_3 is not suitable as a separator for the Ni nanopowder (although we have checked that it does not chemically interact with other nanopowders without Ni, for example, the FeCo powder). A nanodiamond powder can be proposed as an alternative. When using it as a spacer for the Ni nanoparticles, results for synthesis and the morphology of the carbon coverings are similar to the above-described ones, but it does not chemically interact.

Table 3. Comparison of the nominal thicknesses of the initial permalloy films and the thicknesses thereof measured by X-ray reflectometry

Sample	Measured thickness, Å
55	50
105	105
300	290
500	475

2.4. Ensemble of the nanoparticles on the substrate

Experiments of synthesis of graphene and other carbon coatings are often carried out on an ensemble of isolated nanoparticles on the substrate surface. This approach inherently excludes sintering as well as chemical interactions due to absence of a spacer powder. It was previously [8,27] shown that during chemical deposition of carbon the thin epitaxial film is ruptured into separate particles and the covering is synthesized on these particles. Clusterization is caused by melting or softening of the film and poor wetting of the dielectric substrate with a metal.

Hereinafter, we will designate the samples by a thickness of the initial permalloy film. For example, the „sample 15“ means the Al_2O_3//Py(15 Å)/C system, where C is a carbon nanostructure formed on the surface.

X-ray studies of the considered samples were carried out. They included methods of X-ray reflectometry and X-ray diffraction in a grazing beam. The measurements were performed in the laboratory X-ray diffractometer Empyrean (the Institute of Metal Physics, Ural Branch of the Russian Academy of Sciences, Yekaterinburg). Radiation used is the line CoK_α, a weighted average wavelength is 1.79 Å.

Verification of the initial permalloy films by X-ray reflectometry showed good structural perfection of the films and that their real thicknesses are close to the nominal values. All the reflectivity curves (Fig. 7, *a*) exhibit clear oscillations, thereby indicating good smoothness both of the film surface and a boundary with the substrate. The film thicknesses that are determined by the Fourier-analysis express method are shown in Table 3 as compared to the claimed values. It is clear that the differences are not critical. The data for the sample 15 are not obtained due to lack of the material for X-ray study.

When trying to perform the reflectometry study of the samples after synthesis of the carbon covering, we have found a sharp decrease of intensity of reflection without any oscillations (Fig. 7, *b*), which indicates significant increase

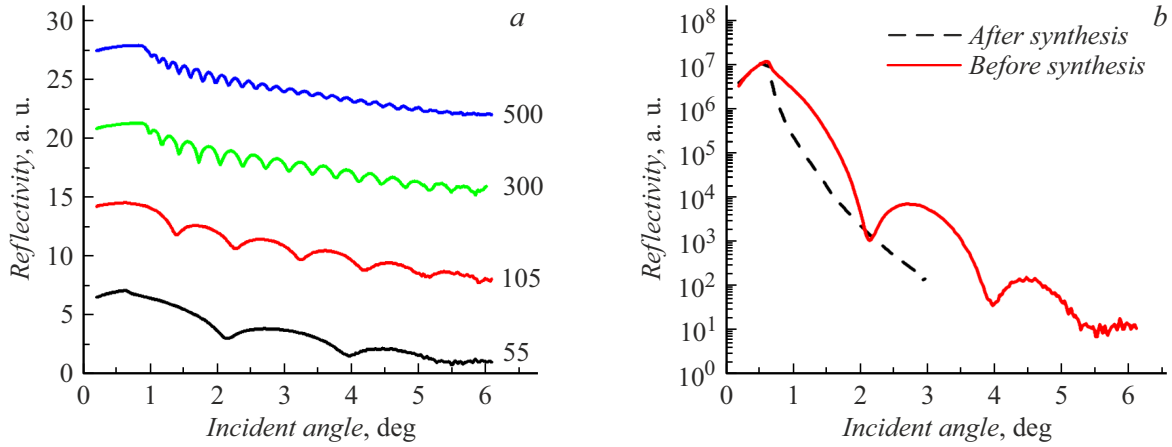

Figure 7. Reflectometry curves of the Al_2O_3//Py(t Å) samples: a — the initial permalloy films before synthesis of the carbon covering (the graphs are shifted along the vertical axis for clarity); b — comparison of the curves before and after synthesis of the carbon covering as exemplified by the sample 55.

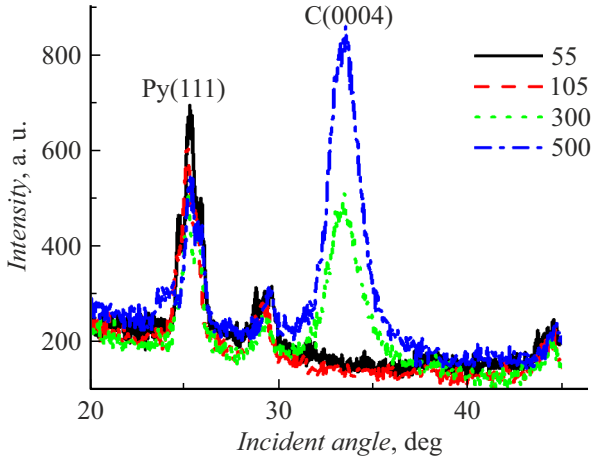

Figure 8. X-ray diffraction patterns of the studied samples, which are obtained in the grazing beam.

of roughness of the surface of the studied films, which is related to formation of the nanoparticles.

The X-ray diffraction patterns in the grazing beam exhibit quite intense carbon peaks (0004) on the samples 300 and 500 (Fig. 8). It indicates presence of clusters or grains of multi-layer graphene or graphite. A typical size of these particles as estimated by the FWHM (full width at half maximum) is ~ 30 Å.

Fig. 9 shows optical microphotos of the surface of the studied samples (a size of the spot is $190 \times 250\,\mu$m). For the samples 15 and 55, the surface looks smooth and has not pronounced specific features. Triangular items are substrate defects and not related to the carbon covering. The samples 105, 300 and 500 exhibit graininess of the surface, thereby indicating formation of the nanoparticles. With increase of the permalloy thickness, the spots become clearer and their distribution is more uniform. The sample 105 also exhibits large smeared dark spots, whose nature is not entirely clear. Apparently, they are specific features of the initial Al_2O_3 substrate.

The surface of the samples was analyzed by atomic-force microscopy (AFM). The instrument is an atomic-force microscope Solver Next (the Institute of Metal Physics, Ural Branch of the Russian Academy of Sciences, Yekaterinburg). For comparison, it included scanning of the initial permalloy films; the films after annealing in hydrogen; the films after synthesis of graphene (Fig. 10).

The AFM images of the initial films practically do not change with the thickness. „Steps“ of a vicinal surface $(1\bar{1}02)$ of sapphire are clearly seen, this surface is also designated as the r- plane. They become poorly discernable for the sample 500, which is related to the large thickness of the permalloy layer that starts smoothing irregularities of the sapphire substrate. Several bright points on the left on the image for the sample 55 are contaminants that will be removed during annealing before synthesis of graphene. The root-mean-square roughness of the surface is approximately the same for all the samples and is 0.4–0.5 nm. The profiles of the surface are shown in Fig. 11, a.

For the sample 15 the picture is not substantially changed after annealing, but one can notice small light dots that are uniformed spread across the surface. The root-mean-square roughness of the surface is a bit increased approximately to 0.5–0.6 nm. After synthesis of the carbon covering, the surface exhibits multiple fine round particles that are uniformly distributed. They are so frequent that they seem to merge with each other but do not form larger clusters due to a different height.

Fig. 11, b shows the profiles of the surface of the films after annealing. For the sample 15, the roughness is so low that its profile is not visible among the others. For the samples 55 and 105, the peaks caused by the nanoparticles have a quite sharp top, which can indicate their near-spherical form. For the samples 300 and 500, the top of

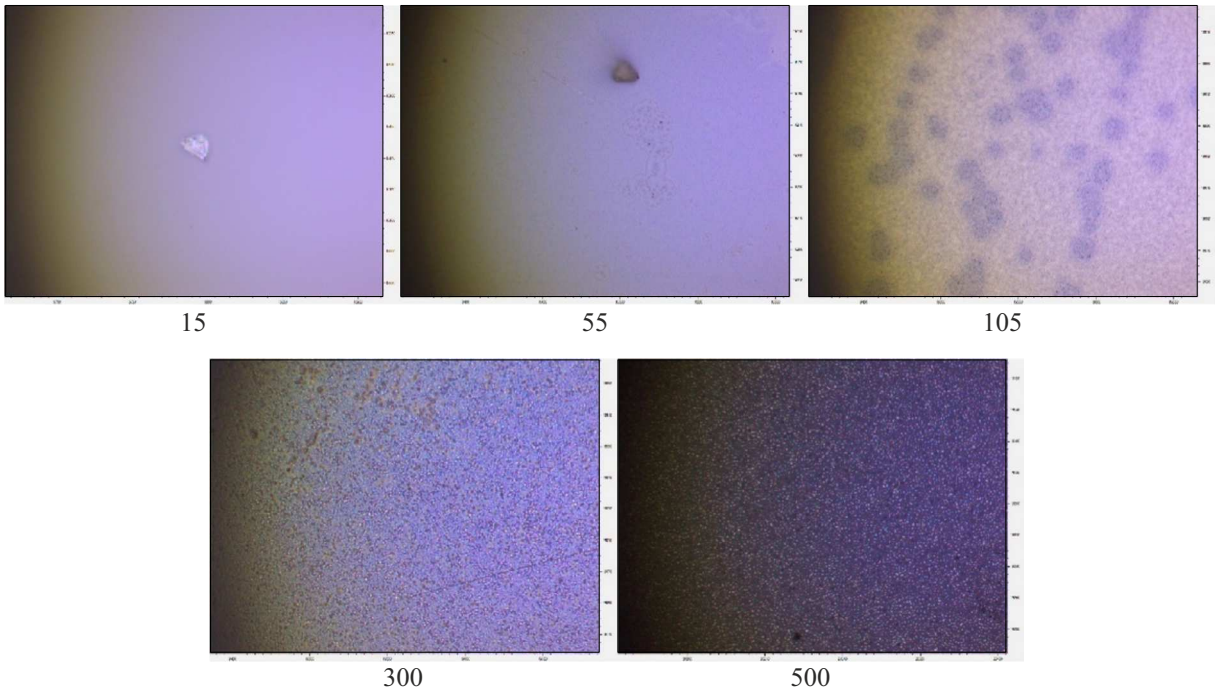

Figure 9. Optical microphotos of the surface of the studied samples.

Table 4. Averaged characteristics of the nanoparticles that are formed at the various stages of synthesis

Sample	After annealing			After synthesis		
	Form	Sizes, nm	Height, nm	Form	Sizes, nm	Height, nm
15	No particle observed			Circles	45–60	2.5
55	Circles	65–140	12	Circles	80–160	14
105	Squares	70–230	27	Squares	250–350	31
300	Circles, elongated hexagons	600 × 800	69	Hexagons	900 × 1500	90
500	Ovals, elongated hexagons	800 × 1300	110	Ovals, rectangles	1100 × 1700	89

the peaks originates a plateau, whose width is comparable with the peak height. It is typical for a cubic form of the particle. The average sizes of the obtained nanoparticles, which are determined by the AFM images, are shown in Table 4.

So, there is clusterization of the film after annealing and it forms many particles. On average, the particle sizes increase with increase of the thickness of the initial film. With the small thicknesses, the nanoparticles have a near-spherical form. For the bigger thicknesses (300 and 500), some particles get a flat top. As the particles grow, so do the distances between them.

After synthesis of the carbon covering, the particles still increase a bit in sizes, so does the height, which is related to formation of the carbon film on them. The exception is the sample 500 (Table 4), whose average height of the particles above the film surface is reduced after synthesis.

The permalloy has a cubic face-centered lattice. When miniature drops are crystallized, they can take a form that is dictated by a symmetry of the lattice. Consequently, we observe the square- and hexagonal-shaped particles depending on its orientation. If two particles are near each other and merge during growth, they can form an elongated hexagon. If resolution of a microscope is not enough to discern angles, then we will see a circle or an oval, respectively,

The Raman spectra for all the studied samples are shown in Fig. 12.

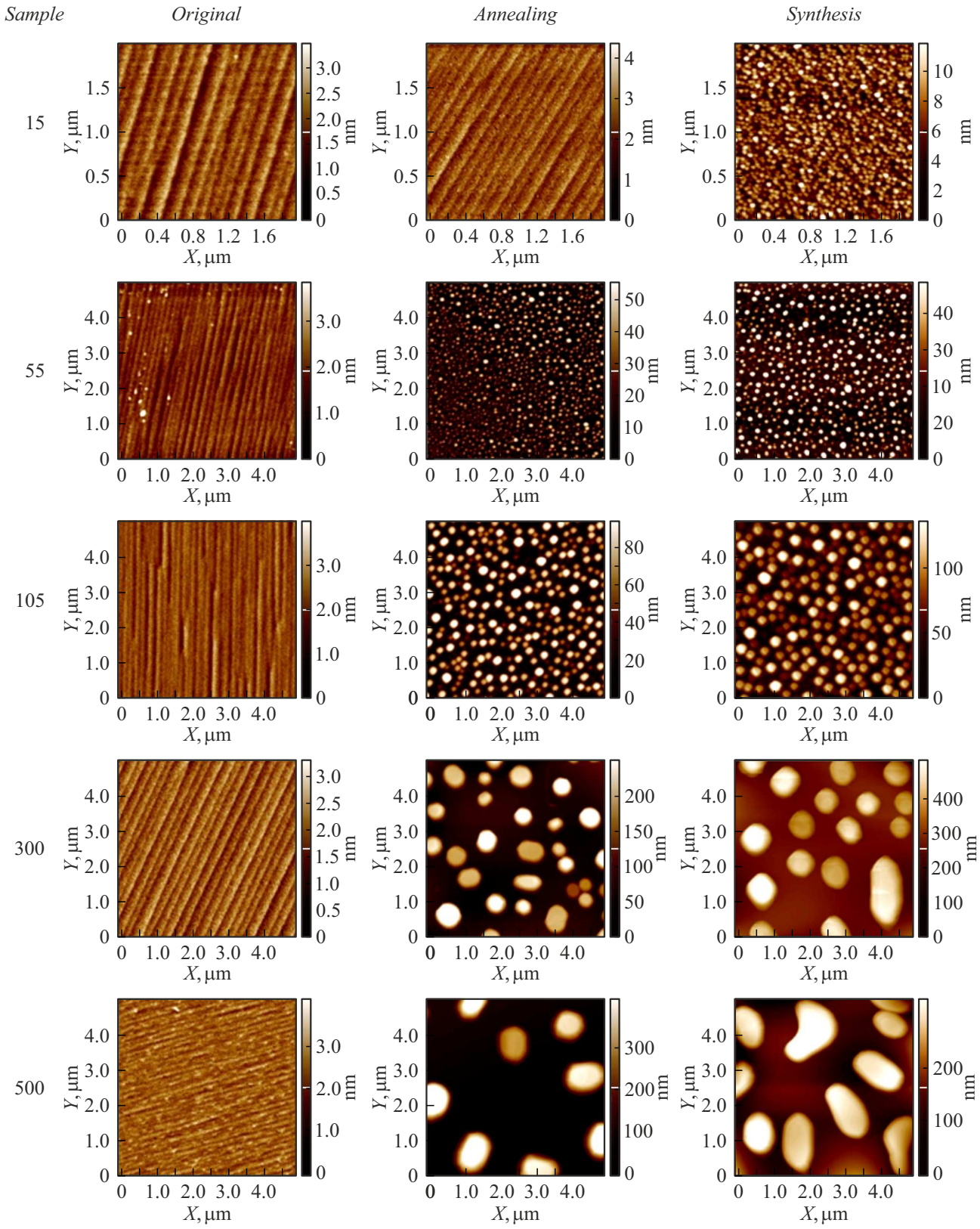

Figure 10. Images of the surface of the studied films, which are obtained by the AFM method. The image size is $5 \times 5\,\mu$m. For the sample 15 the size is $2 \times 2\,\mu$m.

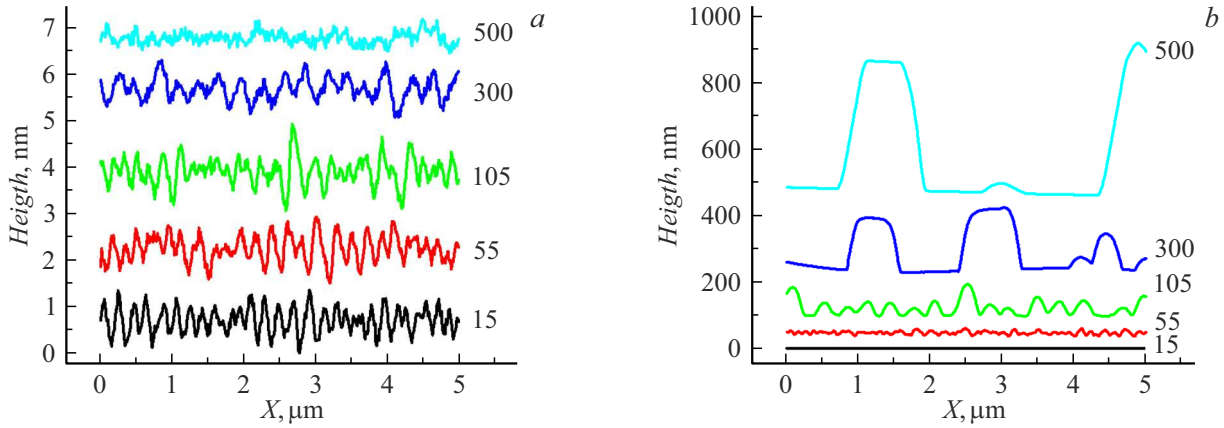

Figure 11. Profiles of the surface of the Al_2O_3//Py substrates before annealing (a) and after annealing (b).

Table 5. Characteristics of the peaks of the Raman spectra for the samples 105 and 300

Sample	Position of the peak G, cm^{-1}	FWHM of the peak $2D$, cm^{-1}	I_D/I_G	Position of the peak $2D$, cm^{-1}	FWHM of the peak $2D$, cm^{-1}	I_{2D}/I_G
105	1585	63	~ 1.9 high density of defects	2681	90 multi-layer graphene	~ 0.6 multi-layer graphene
300	1571	26	~ 0.01 very low density of defects	2689	74 multi-layer graphene	~ 0.8 multi-layer graphene

For the sample 15, the spectrum is heavily noisy and has low-intensity peaks. It is related to a small thickness of the permalloy film. According the above-described mechanism, this film could dissolve only a small amount of carbon, which was later released on the surface during cooling. In turn, the small amount of carbon on the surface resulted in a weak Raman signal. Nevertheless, it is possible to discern the peak G on the spectrum, which indicates presence of an ordered carbon covering, rather than an amorphous one. The peak $2D$ is much higher than the peak G, it is wide and consists of at least two components (possibly, three ones, but a low signal-to-noise ratio does not make it possible to readily identify the third component). This kind of spectrum is typical for multi-layer graphene [28] with quite strong defectiveness. Taking into account the small amount of the material, it can be assumed that the multi-layer graphene formed separate islands, between which amorphous carbon or a pure permalloy film is arranged.

The Raman spectrum for the sample 55 has the peak $2D$ of the same height and structure, which makes it possible to assume that there is multi-layer graphene. The peaks G and D are higher, which can be due to the large amount of the material as compared to the sample 15. The intensity ratio $I_D/I_G = 1.34$ is lower than for the sample 15 ($I_D/I_G = 1.97$) and the produced graphene is less defective. The peak G exhibits slight asymmetry, which is related to emergence of the peak D', which also describes defectiveness of the carbon covering.

As shown above, the sample 105 has dark and light spots that are visible on the microphoto. One's own kind of the Raman spectrum is typical for each type. The spectra in the dark spots to the fullest extent correspond to the spectra of multi-layer nanographene or nanographite [28], i.e. these spots must have formed graphene „stacks“, which had nanometer transverse sizes and open edges. In the light spots of the sample 105, the spectrum peaks have noticeable high intensity and correspond to highly defective multi-layer graphene.

The spectrum of the sample 300 is characterized by absence of the peak D and symmetry of the peaks G and $2D$. Multi-layer (the number of the layers exceeds 5) graphene of high structural perfections is formed on this film. The spectrum of the light spots of the sample 105 and the spectrum of the sample 300 were additionally analyzed using the Lorentz function and the obtained parameters are

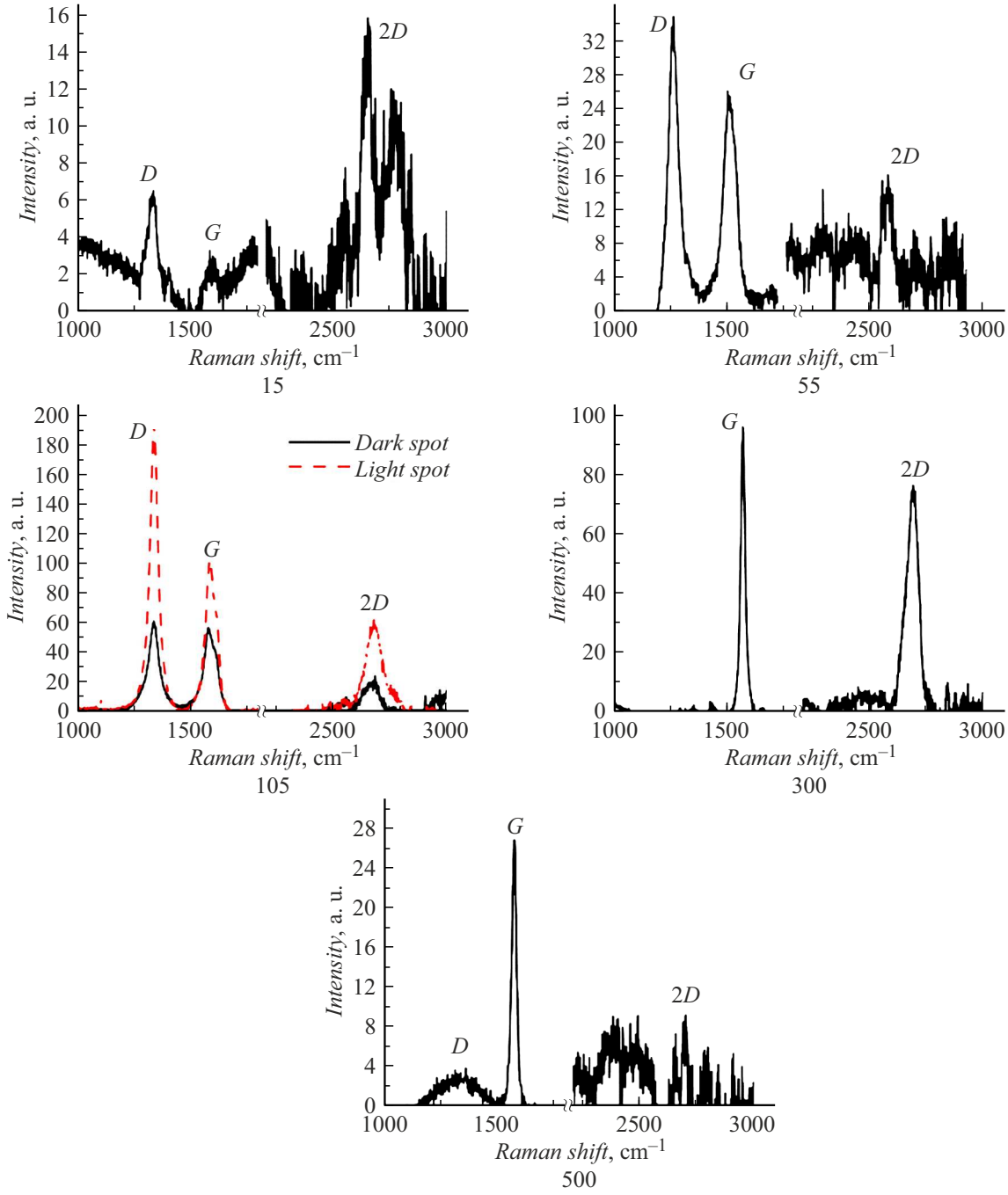

Figure 12. Raman spectra of the studied samples.

shown in Table 5. The Raman spectrum for the sample 500 corresponds to graphite with a small number of defects.

The carbon layers „envelope“ the nanoparticles on the substrate and in case of the large thicknesses of the initial films they fill a space between them. It follows from the AFM experiments — for the samples 300 and 500 the height of the „background“ (the space between the particles) is non-zero according to a microscope scale. For the same samples, X-ray diffraction in the grazing beam detects a clear carbon peak that corresponds to the plane (0004) that is parallel to the substrate surface. No such peak is observed for the systems with the smaller initial thickness. Whence, it can be concluded that multi-layer graphene (graphite) is present between the particles in a noticeable amount. The carbon nuclei that grow on the various particles turn out to be quite large to clump together. In case of the sample 300, „hanging“ multi-layer graphene can be also formed, whose „supports“ are the islands, but this hypothesis requires further examination. This assumption can be supported by no peak *D* on the Raman

spectrum of this sample, since when several nuclei combine, the boundaries between them shall increase defectiveness of the carbon layers.

Structural perfection of the coverings demonstrate a certain dependence on the initial film thickness. With the small thicknesses, we have produced multi-layer graphene with a high density of defects. It is related to its localization on the particles (and, respectively, significant deviation of its geometry from the planar one) and presence of large areas uncovered by carbon. At the thickness 300, an almost defectless covering is formed. But with further increase of the thickness and a transition of multi-layer graphene into graphite, defectiveness starts slightly growing, which is related to combination of the nuclei from the different particles.

Conclusion

It is shown that the chemical vapor deposition method can be used to form carbon coatings that are multi-layer graphene, both on metal and dielectric nanoparticles (in the form of piled powders). In case of using the pure-nickel nanopowders we obtain almost defectless multi-layer graphene. Using the mixture of the nanoparticles „metal + dielectric“, it is possible to prevent sintering, but the carbon coatings originate a small number of structural defects. For the nickel-containing powders, the optimal spacer is nanodiamond, while for other types sapphire Al_2O_3 is suitable.

The influence of the size of the nanoparticles in the ensemble on the substrate (i.e., the influence of the thickness of the initial metal film) on the morphological properties of the carbon covering formed on them has also been systematically analyzed. It is shown that with the small thicknesses of the initial film the carbon covering is localized on the particles, while at the large thicknesses it starts filling the space between them, too. Structural perfection of the coverings is on average higher for the samples with the larger thickness of the metal film. The optimal value of the thickness, which provides a minimum of defects, is ~ 300 Å. At the same conditions of synthesis, for the films with the thickness below 500 Å, the covering is multi-layer graphene, while for 500 Å it is graphite. No amorphous carbon coating was formed.

Funding

The study was carried out under the state assignment of the Ministry of Education and Science of the Russian Federation for the Institute of Metal Physics, Ural Branch of the Russian Academy of Sciences.

Conflict of interest

The authors declare that they have no conflict of interest.

References

[1] S. Bedanta, W. Kleemann. J. Phys. D: Appl. Phys., **42** (1), 013001 (2009). DOI: 10.1088/0022-3727/42/1/013001
[2] O.V. Yazyev, L. Helm. Phys. Rev. B, **75** (12), 125408 (2007). DOI: 10.1103/PhysRevB.75.125408
[3] L.F. Kiss, L. Bujdosó, D. Kaptás. J. Magn. Magn. Mat., **586**, 171217 (2023). DOI: 10.1016/j.jmmm.2023.171217
[4] S. Nakamae. J. Magn. Magn. Mat., **355**, 225 (2014). DOI: 10.1016/j.jmmm.2013.12.018
[5] S. Sharma, R.S. Ningthoujam, N.S. Gajbhiye. Chem. Phys. Lett., **558**, 48 (2013). DOI: 10.1016/j.cplett.2012.12.003
[6] A.V. Eletskii, I.M. Iskandarova, A.A. Knizhnik, D.N. Krasikov. Phys. Usp., **54** (3), 227 (2011). DOI: 10.3367/UFNe.0181.201103a.0233
[7] M. Zeng, Y. Liu, F. Zhao, K. Nie, N. Han, X. Wang, W. Huang, X. Song, J. Zhong, Y. Li. Adv. Funct. Mater., **26** (24), 4397 (2016). DOI: 10.1002/adfm.201600636
[8] Y. Liu, Y. Hu, J. Zhang. J. Phys. Chem. C, **118** (17), 8993 (2014). DOI: 10.1021/jp500751a
[9] M. Sarno, C. Cirillo, C. Scudieri, M. Polichetti, P. Ciambelli. Ind. Eng. Chem. Res., **55** (11), 3157 (2016). DOI: 10.1021/acs.iecr.5b04499
[10] M. Sarno, C. Cirillo, P. Ciambelli. Chem. Eng. J., **246**, 27 (2014). DOI: 10.1016/j.cej.2014.02.014
[11] B. Zhong, A. Mateu-Roldán, M.L. Fanarraga, W. Han, D. Muñoz-Guerra, J. González, L.T. Weng, M.R. Ibarra, C. Marquina, K.L. Yeung. Chem. Eng. J., **435** (1), 134466 (2022). DOI: 10.1016/j.cej.2021.134466
[12] G. Zhao, S. Song, C. Wang, Q. Wu, Z. Wang. Anal. Chim. Acta, **708** (1-2), 155 (2011). DOI: 10.1016/j.aca.2011.10.006
[13] R.J. Fullerton, D.P. Cole, K.D. Behler, S. Das, F. Irin, D. Parviz, M.N.F. Hoque, Z. Fan, M.J. Green. Carbon, **72**, 192 (2014). DOI: 10.1016/j.carbon.2014.02.002
[14] A.H. Lu, W.C. Li, N. Matoussevitch, B. Spliethoff, H. Bönnemann, F. Schüth. Chem. Commun., **1**, 98 (2005). DOI: 10.1039/B414146F
[15] V.A. Tsurin, A.Y. Yermakov, M.A. Uimin, A.A. Mysik, N.N. Shchegoleva, V.S. Gaviko, V.V. Maikov. Phys. Solid State, **56** (2), 287 (2014). DOI: 10.1134/S1063783414020309
[16] A.E. Ermakov, M.A. Uimin, E.S. Lokteva, A.A. Mysik, S.A. Kachevskii, A.O. Turakulova, V.S. Gaviko, V.V. Lunin. J. Phys. Chem. A, **83**, 1187 (2009). DOI: 10.1134/S0036024409070243
[17] V.R. Galakhov, A.S. Shkvarin, A.S. Semenova, M.A. Uimin, A.A. Mysik, N.N. Shchegoleva, A.Ye. Yermakov, E.Z. Kurmaev. J. Phys. Chem. C, **114** (51), 22413 (2010). DOI: 10.1021/jp106612b
[18] E. Butovsky, A. Irzh, B. Markovsky, A. Gedanken. New J. Chem., **36** (1), 155 (2012). DOI: 10.1039/C1NJ20627C
[19] E. Butovsky, I. Perelshtein, A. Gedanken. J. Mater. Chem., **22** (30), 15025 (2012). DOI: 10.1039/C2JM32528D
[20] A.I.Gusev.*Nanomaterialy, nanostruktury, nanotekhnologii* (Fizmatlit,M.,2007) (in Russian).
[21] P. Alvaredo, M. de Dios, B. Ferrari, E. Gordo. *European Congress and Exhibition on Powder Metallurgy. European PM Conference Proceedings* (Reims, France, 2015), p. 1.
[22] Q. Yu, J. Lian, S. Siriponglert, H. Li, Y.P. Chen, S. Pei. Appl. Phys. Lett., **93** (11), 113103 (2008). DOI: 10.1063/1.2982585
[23] H.J. Song, M. Son, C. Park, H. Lim, M.P. Levendorf, A.W. Tsen, J. Park, H.C. Choi. Nanoscale, **4** (10), 3050 (2012). DOI: 10.1039/c2nr30330b

[24] Y. Ueda, J. Yamada, T. Ono, T. Maruyama, S. Naritsuka. Appl. Phys. Lett., **115** (1), 013103 (2019). DOI: 10.1063/1.5098806
[25] A. Dahal, M. Batzill. Nanoscale, **6** (5), 2548 (2014). DOI: 10.1039/c3nr05279f
[26] T. Alves, W.S. Mota, C. Barros, D. Almeida, D. Komatsu, A. Zielinska, J.C. Cardoso, P. Severino, E.B. Souto, M.V. Chaud. J. Mater. Sci., **59** (32), 14948 (2024). DOI: 10.1007/s10853-024-10061-4
[27] X. Zhang, S. Xu, S. Jiang, J. Wang, J. Wei, S. Xu, S. Gao, H. Liu, H. Qiu, Z. Li, H. Liu, Z. Li, H. Li. Appl. Surf. Sci., **353**, 63 (2015). DOI: 10.1016/j.apsusc.2015.06.084
[28] J.-B. Wu, M.-L. Lin, X. Cong, H.-N. Liu, P.-H. Tan. Chem. Soc. Rev., **47** (5), 1822 (2018). DOI: 10.1039/C6CS00915H

Translated by M.Shevelev